

Optical Fiber Pressure Sensor Based on Photoelasticity and its Application

Anbo Wang, *Senior Member, IEEE*, Se He, Xiaojan Fang, Xiaodan Jin, and Junxiu Lin

Abstract—An optical fiber pressure sensor based on the photoelastic effect using a new compensation technique is described in this paper. Two optical sources and a polarization-splitting prism are incorporated into a sensor system to minimize output drifts. The four major factors—the optical source power, the fiber loss, the optical coupling loss, and the modal power distribution in fibers—are well compensated. The measurement range of 0–147 KPa has been obtained with accuracies of 0.2% within the temperature range of -10°C to 42°C and a resolution of 10 Pa has been achieved. Compensation for fiber loss has been observed up to -30 dB. This sensor system has been successfully put into practical operation for oil storage measurement in a tank.

I. INTRODUCTION

SINCE Spillman demonstrated the first extrinsic fiber optic pressure sensor based on the photoelastic effect in 1982 [1], various photoelastic fiber sensors have been fabricated and examined in the laboratory [2]–[5]. Yet, to our knowledge, no one has reported a successful practical application of an extrinsic fiber optic photoelastic sensor for an on-line measurement. The biggest obstacle responsible for this is the long-term stability that is limited by a few factors such as optical loss variations (except for the optical change caused by parameter to be measured). Spillman *et al.* proposed a technique to improve the stability in 1983 [6]. In their method, a polarization beam splitter is incorporated in the sensor head to provide a pair of differential optical output signals that change toward opposite directions with change of measurand. When we take the ratio of the sum of these two signals to the difference between the two signals, the drifts caused by the variations of optical source power and changes in lead-in fiber loss can be significantly reduced. However, the drifts caused by differential changes in the attenuations of the two lead-out fibers, which cannot be tolerated for remote sensing applications, are not removed. Another method was proposed by Culshaw *et al.* in 1985 [7]. In their compensation technique, two optical beam splitters and combiners, such as fiber couplers, were used to compose of an optical bridge. Two light sources, which were connected to the two input legs of

the bridge, and two photodetectors, which were connected to the two output legs of the bridge, were incorporated in the system. The two sources worked alternatively in time. The sensor output was derived, through a specific calculation, from the four output signals of the detectors that correspond to the two sources. In so doing, theoretically, all drifts in this system can be removed. Actually, it is difficult to remove the effects of modal power distribution (MPD) variations in fibers. The most attractive advantage of this method is that it is applicable to most intensity-based fiber sensors. In this paper, a novel compensation technique for polarization-modulated fiber sensors is proposed and experimental results are presented in detail.

II. PRINCIPLE OF OPERATION

For an extrinsic, remote polarization-modulated fiber sensor for absolute measurement, several factors, such as light source power fluctuation, change in fiber attenuation and optical coupling variation between lead-in and lead-out fibers in the optical sensor head cause long-term drifts and limit the accuracy of the sensor. By using the well-known ratio methods, the power variation of the source and the fluctuation of lead-in fiber loss are easily reduced by a few orders of magnitude. However, it is a difficult task to compensate for the coupling variations between the lead-in and lead-out fibers and changes in the lead-out fibers losses because it is not easy to distinguish at the detector ends, the optical power variations that are caused by the measured parameter or by the two factors mentioned earlier when the sensor is used to measure a quasi-static parameter. In this paper we propose a novel technique to solve these problems.

The schematic configuration of a remote fiber optic pressure sensor based on the photoelastic effect is illustrated in Fig. 1. A photoelastic material (PEM) will show a birefringence when a force is applied. Both the polarization axis of a polarizer P and the slow axis of a quarter-wave-plate WP are oriented at 45° to the X axis. A polarization-splitting prism (PS) functions as two polarization analyzers and a beam splitter. The polarization orientation of the linearly polarized transmitted light beam through PS is along the x axis. The polarization orientation of the linearly polarized reflected light beams is perpendicular to that of the transmitted beam.

The light from transmitter T_1 travels along a lead-in fiber F_1 with a loss L_1 to an optical sensor head. After being collimated by a GRIN lens G_1 , the light out of F_1 passes through P , PEM, and WP and is then split by the PS into reflection and transmission beams. The transmission beam is injected into

Manuscript received August 1, 1991; revised May 1, 1992. This work was supported by the National "7.5" Project of the People's Republic of China.

A. Wang was with the Bradley Department of Electrical Engineering, Fiber and Electro-Optics Research Center, Virginia Polytechnic Institute and State University, Blacksburg, VA 24061-0111. He is now with the Department of Applied Physics, Research Institute of Applied Physics, Dalian University of Technology, Dalian 116023, China.

S. He, X. Fang, X. Jin, and J. Lin are with the Bradley Department of Electrical Engineering, Fiber and Electro-Optics Research Center, Virginia Polytechnic Institute and State University, Blacksburg, VA 24061-0111.

IEEE Log Number 9202323.

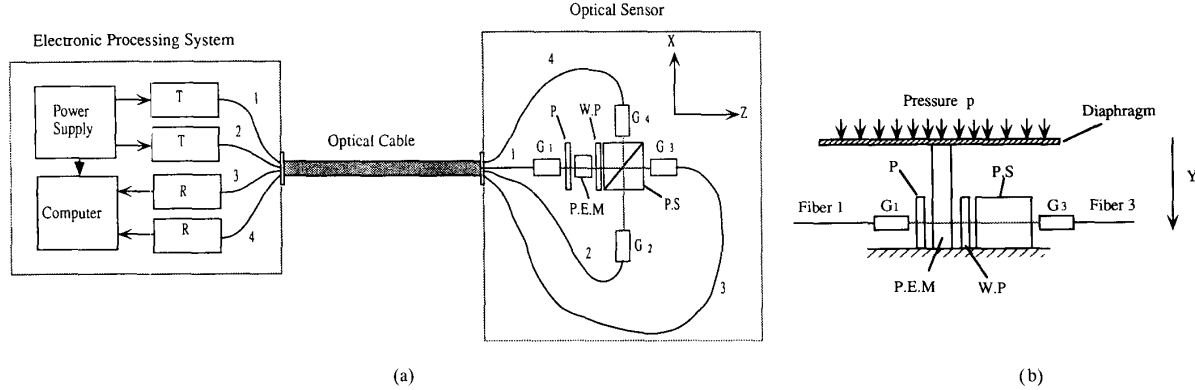


Fig. 1. Schematic of a balance fiber pressure sensor. (a) The compensation principle of the sensor. (b) Side view of the optical pressure sensor head.

a lead-out fiber F_3 by a GRIN lens G_3 and propagates to a photodetector D_1 along F_3 with a loss L_3 . The reflected light is focused into another lead-out fiber F_4 and travels to photodetector D_2 with a loss L_4 . The light from a transmitter T_2 propagates along another lead-in fiber F_2 with a loss L_2 and, after being collimated by a GRIN lens G_2 , is directly splitted by PS into two beams, which are also focused into F_3 and F_4 by G_3 and G_4 , respectively.

For transmitter T_1 , the optical power at the detectors can be written as

$$I_{11} = I_{01} L_1 L_3 \sin^2(\Phi/2 + \pi/4) \quad \text{at } D_1 \quad (1)$$

$$I_{12} = I_{01} L_1 L_4 \cos^2(\Phi/2 + \pi/4) \quad \text{at } D_2 \quad (2)$$

where I_{01} is the optical power of the light passing through the polarizer P , and Φ is the differential phase delay between the linearly polarized X and Y components. It is given by

$$\Phi = 2\pi Cl\sigma/\lambda = 2\pi ClS_e p/(\lambda S_0) \quad (3)$$

where C is the stress-optical coefficient, l is the light propagation length in the PEM, σ is the stress induced by the applied pressure, λ is the wavelength in vacuum, S_e is the effective area of the diaphragm, p is the pressure to be measured and S_0 is the cross-sectional area of the PEM in the X - Z plain. Note that in (3) we have assumed the stress over the light propagation region in the PEM is even. In (1) and (2), we have ignored the coupling losses between the lead-in and lead-out fibers in the sensor head.

When an unpolarized light from a light source, such as an LED, is launched into a multimode fiber, the light out of this fiber is also unpolarized. The sensor described in this paper belongs to this case (see Section III). Thus, for the transmitter T_2 , the power at the detectors can be expressed by

$$I_{21} = 1/2 I_{02} L_2 L_3 \quad \text{at } D_1 \quad (4)$$

and

$$I_{22} = 1/2 I_{02} L_2 L_4 \quad \text{at } D_2 \quad (5)$$

where I_{02} is the output power from T_2 . Note that we have also ignored the coupling losses between the lead-in and lead-out fibers in the sensor head in (4) and (5).

To remove the drifts caused by the factors mentioned in Section I, a parameter S is defined in the following expression.

$$S = (I_{11}/I_{21} - I_{12}/I_{22}) / (I_{11}/I_{21} + I_{12}/I_{22}) \\ = \sin[2\pi ClS_e p/(\lambda S_0)]. \quad (6)$$

Equation (6) indicates the fact that S is independent of the fiber losses and the output powers of the light sources. It is further understood that S is also independent of the two photodetector responsivities and the amplifier gains. On the other hand, since the parameters for the two receiving channels—the GRIN lenses and lead-out fibers, which are composed of G_3 and F_3 as well as G_4 and F_4 , are the same, the ratio I_{11}/I_{21} or I_{12}/I_{22} is immune to the modal power distribution (MPD) in the lead-in fibers. Also, the parameters—the GRIN lenses and lead-in fibers—for the two lead-in channels, which are composed of G_1 and F_1 as well as G_2 and F_2 , are the same, the MPD, in F_3 or F_4 , excited by the two light sources, respectively, are close to each other. Thus the propagation lights, which are from T_1 and T_2 , respectively, in F_3 or F_4 carry almost the same information of the fiber loss and its variations. Therefore, a remote fiber-optic pressure sensor with high stability and accuracy is expected.

III. EXPERIMENTS

The schematic of the experimental setup is shown in Fig. 1. Two light-emitting diodes (LED's) with central wavelengths of $0.85 \mu\text{m}$ were used as the light sources in order to reduce modal noise [8] and the photodetectors were two pigtailed Si-P-i-n photodiodes. The photoelastic material was made of quartz glass strip with dimensions of $3 \times 12 \times 3 \text{ mm}^3$. The force was exerted on the photoelastic material along the largest dimension (Y axis). The diaphragm diameter was 55 mm. The optical sensor was connected to an electronic processing system by a 250-m long optical cable that contained four $100 \mu\text{m}$ -core graded-index glass fibers with numerical

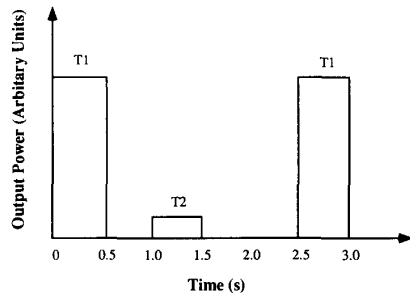


Fig. 2. LED work order in time.

apertures of 0.24. To ensure data processing accuracy, two highly accurate digital voltmeters with five showing digits were chosen as A/D converters and a microcomputer was programmed to process the converter outputs automatically. In order to separate the signals from the different sources, the microcomputer controlled the two LED's such that they worked alternatively in time, as is shown in Fig. 2. A pneumatic pressure source provided the pressure during the calibration procedure. The curve of the calibration results as shown in Fig. 3 demonstrates that the sensor had linear outputs with applied pressure ranges of 0–147 KPa. To determine the sensitivity of this sensor system, 100 outputs of the sensor were recorded continuously without pressure applied to the sensor. The standard deviation σ of this group data was found to be 3.25 Pa. Then, this sensor sensitivity, which was given by 3σ was determined to be 10 Pa. It is believed that higher sensitivity could be obtained by increasing the digits of the two A/D converters. The theoretical sensitivity limited by quantum noise (shot noise) has been calculated to be 0.5 Pa [9]. The stability of a remote absolute fiber sensor is usually affected by such factors as fiber loss variations, the MPD in fibers, and the sensor temperature, etc. A few tests are described as follows to check the practical applicability of the system.

A. Effects of Fiber Losses and MPD

As we know, the output of an intensity-based fiber usually depends on the attenuation of the fiber involved in this sensor. Also, for a given multimode optical fiber, the intensity pattern at the output endface of the fiber, and hence at far-field cross sections, is determined by both the MPD and the phase delay of the guided modes in the fiber. When a low coherence light source such as an LED is used, the effect of the phase delay of the modes becomes almost negligible. Thus the near- and far-field field patterns are uniquely determined by the MPD. Because any optical fiber coupling system like the optical sensor head shown in Fig. 1(a) can be equivalently considered as a spatial filter, the output of an extrinsic multimode fiber optic sensor may also be dependent on the MPD in fibers that the sensor uses. These two effects—fiber loss and MPD—usually pose a serious challenge to practical operations of intensity-based optical fiber sensors.

For the evaluation of the dependence of the fiber sensor just described on fiber loss and MPD, large changes of fiber

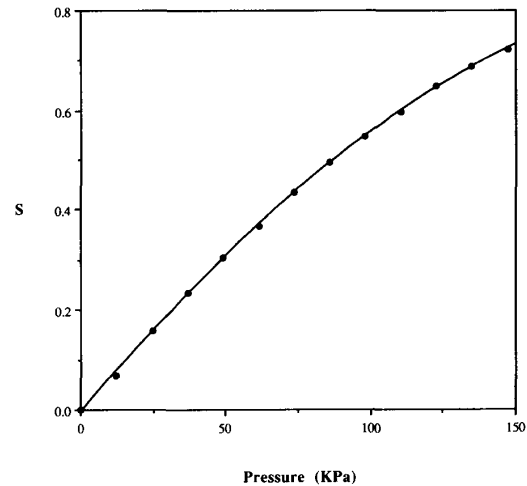


Fig. 3. Sensor output versus applied pressure.

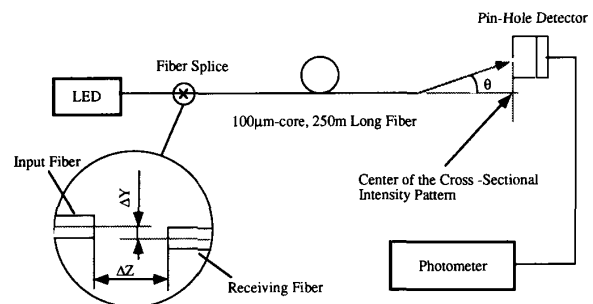


Fig. 4. Experimental setup for the measurement of the modal power distribution.

loss and MPD are necessary. In this experiment these changes were provided by changing the longitudinal gap ΔZ or the lateral offset ΔY between the two fiber endfaces at a fiber splice as shown in Fig. 4. However, the problem is that the optical power and MPD in the receiving fiber of the splice vary simultaneously when ΔZ or ΔY is changed, and this effect makes it difficult to separately evaluate drifts caused, respectively, by fiber loss variations and MPD variations. To roughly separate the drifts induced by these two parameters, it is necessary to know how the MPD in the fiber depends on ΔZ and ΔY . For a multimode optical fiber, there are two waveguide theories derived from the ray optics and wave optics, respectively. One of the correlation between the two theories is that high-order modes in the mode theory from the wave optics correspond to the optical rays propagating in the fiber with large angles with respect to the longitudinal axis of the fiber [10]. Hence, at the output of the receiving fiber, high-order modes contribute more to the outer area of a cross-sectional far-field radiation pattern than low order modes do. So, this far-field intensity pattern carries the information of the MPD in the receiving fiber. The experimental setup shown in Fig. 4 was constructed to measure the dependence of the far-field intensity pattern, which is relative to the MPD in the receiving fiber, on ΔZ or ΔY . The results shown in

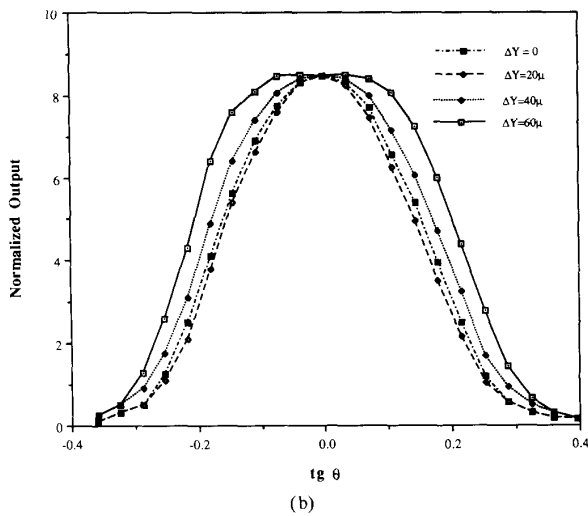
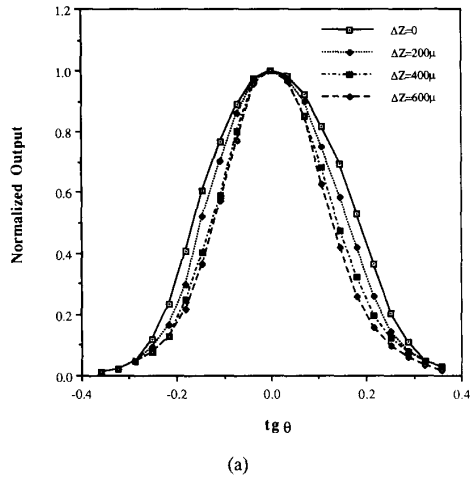


Fig. 5. Dependence of the far-field intensity distribution on (a) the axial gap and (b) the radius offset.

Fig. 5(a) indicate that the normalized cross-sectional intensity profile at far-field became thinner and thinner with the gradual increase of ΔZ . This phenomenon implies that the optical power distributed on high-order modes in the receiving fiber decreased with the increase of ΔZ . In Fig. 5(a), it is noted that the MPD tended to be stable as ΔZ was over $400 \mu\text{m}$. In Fig. 5(b), we see that the far-field intensity profile became fatter and fatter with the increases of ΔY . This observed phenomenon indicates that the MPD in the receiving fiber sharply changed with the increase of ΔY . It seemed reasonable to determine ΔZ at $400 \mu\text{m}$ as the starting point from which we began to increase the longitudinal gap to provide optical losses approximately without the MPD variations. The variation of ΔZ from 0 to $400 \mu\text{m}$ or change in ΔY can be used to evaluate the dependence of the sensor output on the MPD. In doing so, results of the sensor output versus fiber losses could be approximately achieved. Fig. 6 demonstrates that the output fluctuations of the sensor remained within 0.1% with fiber losses up to -30 dB . However, the outputs of the sensor

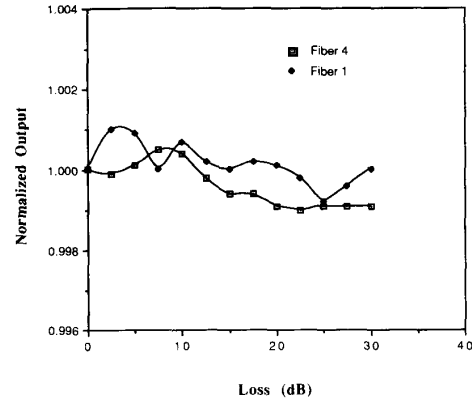


Fig. 6. Sensor output as a function of fiber loss.

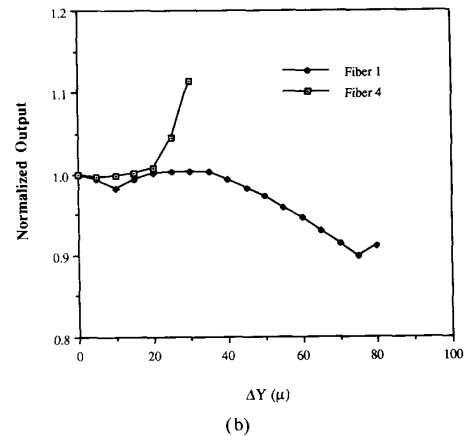
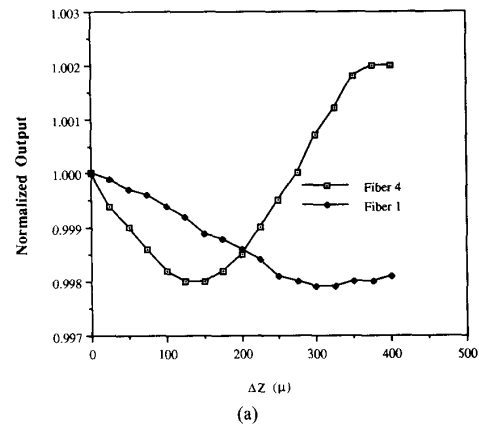


Fig. 7. Dependence of the sensor output on (a) the axial gap and (b) the radius offset.

changed much more than 0.1%, as shown in Fig. 7 when ΔZ was varied from 0 to $400 \mu\text{m}$ (this process caused about 3 dB optical power variation) or ΔY changed from 0 to $60 \mu\text{m}$. After comparing the results presented in Fig. 6 with those shown in Fig. 7, it can be concluded that the output changes of the system, shown in Fig. 7, were mainly caused by the

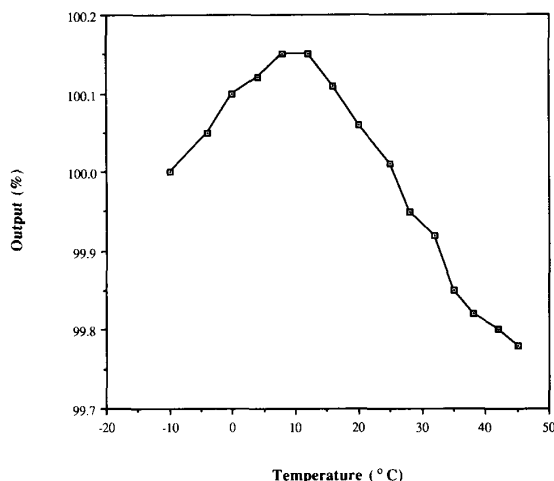


Fig. 8. Temperature effects on sensor output.

MPD variations. But when the optical fiber cable is placed and fixed outside, the MPD variations in the fibers, caused by temperature changes, are expected to be much smaller than those caused by the fiber splice changes shown in Fig. 7 (see Section III-B).

B. Temperature Effects

1) *Optical Sensor Head:* During the experimental evaluation of temperature effect of the optical sensor head, the sensor head as shown in Fig. 1(a) was placed in a temperature chamber whose temperature was monitored using thermocouple and the temperature variation rate was controlled manually within 3°C/h in order to let the optical components in the sensor head catch up with the temperature change in the temperature chamber. The sensor outputs and the temperatures were periodically printed out by a printer linked to the microcomputer that processed the sensor outputs automatically. Fig. 8 displays the experimental results and shows that the sensor output fluctuations were within 0.2% with the temperature ranging from -10 to 45°C (over this temperature change, the relative optical power variations at the two photodetector ends were up to about 40%).

2) *Optical Cable:* In practical uses of remote fiber optic sensors for absolute measurements, the optical cable linking the sensor to the electronic processing system usually has to be placed outdoors. In these cases the optical cable temperature, which can cause changes of both fiber loss and MPD, is highly dependent on the outside temperature. The temperature effect of the optical cable was tested experimentally to check the feasibility of this sensor system for practical use. In the experiment, the 250-m-long optical cable was placed in a temperature chamber. The outputs of the sensor and the temperature from the thermocouple were simultaneously recorded. A high stability of 0.05% was obtained with a temperature range of 12–46°C. In addition, the output of the sensor system did not show any change, within the experiment accuracy of 0.02, when either of the photodetectors was heated up to about

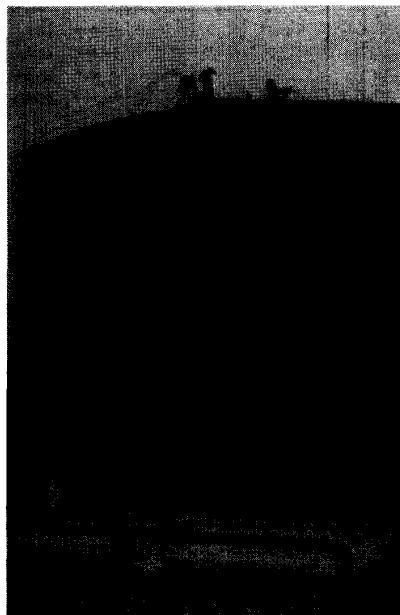


Fig. 9. Photograph of the oil tank.

60°C or when the gain of the preamplifiers was changed by a factor of 10.

IV. APPLICATION

The sensor system just described was applied to measure the storage of crude oil in a crude oil tank. The tank, shown in Fig. 9, was 15 m high and 31 m in diameter. In order to detect the oil pressure, the sensor was installed at the bottom of the tank as shown in Figs. 10 and 12. The electronic processing system, shown in Fig. 11, was located in a control room that was 200 m away from the tank. For an ideal cylindrical tank, the oil storage W is given by

$$W = pS_c \quad (7)$$

where S_c is the cross-sectional area of the tank and p is the differential pressure between the top (the gas state) and the bottom (the liquid state) of the tank. Given S_c , the storage can be derived from the differential pressure. In practice, oil tanks are not ideal cylinders and a small modification has to be made. In order to examine the stability of the sensor system under in situ operation conditions, the input and output valves of the tank were closed to keep the storage of the tank a constant. The liquid level of 9.5 m had been kept to a constant for 15 h. The sensor output was printed out periodically. The stability of the sensor was measured to be 0.16% over this 15 h. Over a one-year test operation of the fiber-optic sensor system under the in situ conditions, the measured results from the fiber-sensing system were compared with the results obtained periodically using the conventional method. The conventional method can be divided into two steps. First, the oil level in the tank was manually measured by using a ruler through a measurement hole on

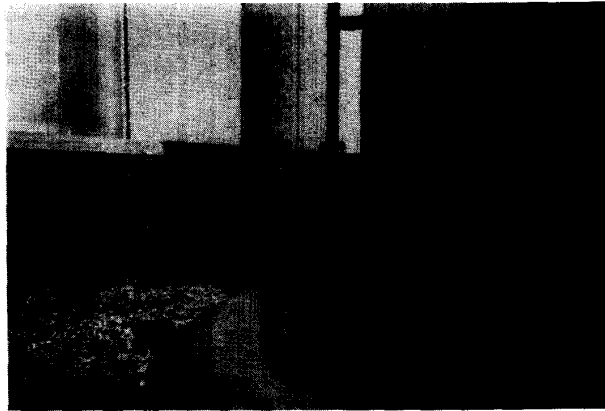


Fig. 10. Optical sensor connected to the tank.

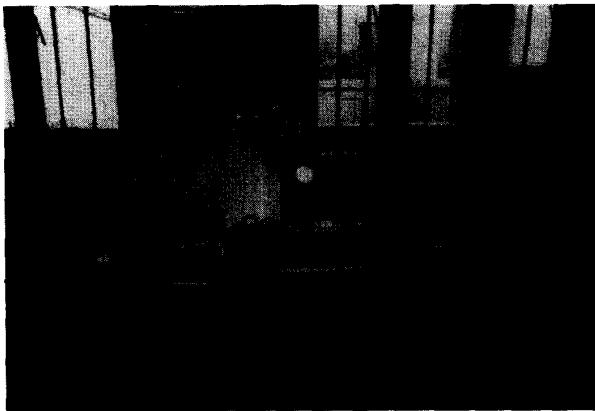


Fig. 11. Electronic processing system located in the control room.

the top of the tank. The liquid volume V in the tank could be achieved by referencing a volume table, made form the calibration of the tank, with the measured liquid level. Second, three samples of the oil in the tank were taken at three different relative vertical levels (100, 50 and 5%), respectively. The temperature of these samples is recorded simultaneously. The

average density of the oil at laboratory temperature is obtained by using a specific technique. This average density value at the laboratory temperature was then transformed to the density value D at the real averaged temperature of the tank. The oil storage of the tank was given by the formula $W = DV$ based on the conventional method. Over this one-year operation of the fiber-optic sensing system under the in situ conditions, the periodic comparisons between the measured results from the fiber sensor system and from the convention method indicated that a high accuracy of 0.25% had been obtained.

V. CONCLUSION

A practical optical fiber-pressure sensor system based on photoelasticity using a novel compensation technique has been described. The system has a pressure measurement range of 0–147 KPa with a sensitivity of 10 Pa. It maintained a high accuracy of 0.2% regardless of the fiber losses up to –30 dB and regardless of the temperature changes from –10 to 42°C. The system has superior abilities to compensate for the large variations of MPD in the fibers. This sensor has been successfully applied to measure storage in a crude oil tank and a high accuracy of 0.25% has been obtained under the in situ operation conditions over the one-year test use. The

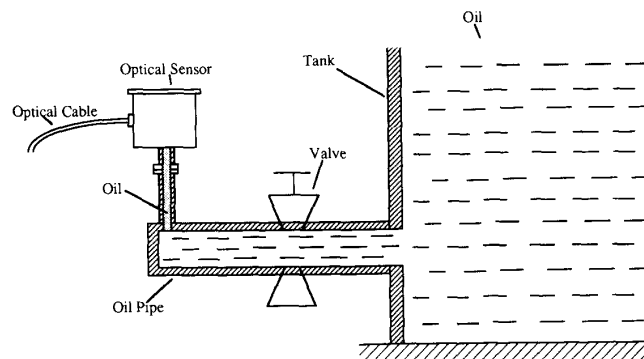


Fig. 12. The installation of the optical sensor to the tank.

compensation method proposed here is also applicable to other extrinsic polarization-modulation fiber sensors.

ACKNOWLEDGMENT

The authors would like to thank the Liao He Bureau of Petroleum for their cooperation.

REFERENCES

- [1] W. B. Spillman, Jr., "Multimode fiber-optic pressure sensor based on the photoelastic effect," *Opt. Lett.*, vol. 7, no. 8, pp. 388-340, 1982.
- [2] B. E. Jones and R. C. Spooncer, "Photoelastic pressure sensor with optical fiber links using wavelength characterization," in *Proc. Conf. Opt. Fiber Sensors OFS'83 (London)*, 1983, pp. 173-177.
- [3] G. Martens, "Photoelastic fiber-optic sensors for the measurement of force and pressure" *Technisches Messen tm*, vol. 53, Jahrgang, Heft 9/1986.
- [4] A. Wang, Z. F. Liu, B. Wu, S. He, H. L. Qi, J. L. Yao, and J. X. Lin, "An optical fiber sensor system for measuring oil storage in tank," in *Proc. Conf. Opt. Fiber Sensors OFS'86 (Tokyo, Japan)*, 1986, pp. 319-322.
- [5] S. Tai, K. Kyuma, and M. Nunoshita, "Fiber-optic acceleration sensor based on the photoelastic effect," *Appl. Opt.*, vol. 22, no. 11, pp. 1771-1774, 1983.
- [6] W. B. Spillman, Jr. and D. H. McMahon, "Multimode fiber optic sensor," in *Proc. Conf. Opt. Fiber Sensors OFS'83 (London)*, 1983, pp. 160-163.
- [7] I. P. Giles, S. McNeill, and B. Culshaw, "A stable remote intensity based fiber sensor," *J. Phys. E: Instrum.*, vol. 18, pp. 1124-1126, 1985.
- [8] A. Wang, B. Wu, S. He, and J. X. Lin, "Theoretical and experimental study of modal noise for non-function fiber sensors," *Opt. Commun. Technol. (Chinese)*, vol. 12, no. 1, pp. 27-31, 1988.
- [9] A. Wang, "Fiber optic pressure sensor with high accuracy and its applications," Ph.D. dissertation, Dalian University of Technology, People's Republic of China, pp. 72-74, 1989.
- [10] T. Okoshi, *Optical Fibers*. New York: Academic Press, 1982, ch. 2.



Anbo Wang (M'91) received the B.S. degree from Anshan Institute of Technology, China. He received the M.S. and Ph.D. degrees from Dalian University of Technology, China, in 1986 and 1989, respectively.

He has been working in the field of fiber-optic components and sensors since 1985. He joined the faculty of Applied Physics at Dalian University of Technology in 1986. Currently, he is working, as a Research Scientist, at the Fiber & Electro-Optics Research Center in the Bradley Department of Electrical Engineering at Virginia Polytechnic Institute and State University. He has authored and coauthored more than 50 papers in the field of fiber-optic components, devices and sensors, and holds two patents.

Dr. Wang is a member of the OSA.

Se He, photograph and biography not available at the time of publication.

Xiaojan Fang, photograph and biography not available at the time of publication.

Xiaojan Jin, photograph and biography not available at the time of publication.

Junxiu Lin, photograph and biography not available at the time of publication.